Strain-driven phase boundaries in $BiFeO_3$ thin films studied by atomic force microscopy and x-ray diffraction

Heng-Jui Liu,[2,3] Chen-Wei Liang,[1] Wen-I Liang,[1] Hsiang-Jung Chen,[1] Jan-Chi Yang,[1] Chun-Yen Peng,[1] Guang-Fu Wang,[4] Feng-Nan Chu,[4] Yi-Chun Chen,[4] Hsin-Yi Lee,[3] Li Chang,[1] Su-Jien Lin,[2] and Ying-Hao Chu[1]

[1]*Department of Materials Science and Engineering, National Chiao Tung University, Hsinchu 30010, Taiwan*

[2]*Department of Materials Science and Engineering, National Tsing Hua University, Hsinchu 30013, Taiwan*

[3]*National Synchrotron Radiation Research Center, Hsinchu 30076, Taiwan*

[4]*Department of Physics, National Cheng Kung University, Tainan 70101, Taiwan*

(Received 26 June 2011; revised manuscript received 8 December 2011; published 17 January 2012)

We report a detailed study on the strain-driven phase transition between the tetragonal-like and rhombohedral-like phases in epitaxial $BiFeO_3$ (BFO) thin films which focuses on their structural nature, thermodynamic stability, and ferroelectric/piezoelectric properties. We first show that the tetragonal-like phase, which has a large *c/a* ratio ($\sim$1.2), in the compressively strained BFO is thermodynamically more favorable at high temperature and high strain state (small thickness). We also report a phase transition between two monoclinic phases at 150 °C. The two monoclinic phases are differentiated by their *c*-axis parameters and tilting angles: The low-temperature phase (M_C) has a *c*-axis parameter of 4.64 Å and a tilting angle ($\beta = 88.5^\circ$) along the *a* axis, while the high-temperature phase (M_A) has a *c*-axis parameter of 4.66 Å and a tilting angle ($\beta = 86.8^\circ$) along both of the *a* and *b* axes. We further show that samples undergoing the M_C–M_A phase transition exhibit ferroelectric polarization rotation and piezoelectric enhancement. Our findings directly unveil the close links between structural changes, polarization rotation, and large piezoelectricity at morphotropic phase boundaries in $BiFeO_3$.

DOI: 10.1103/PhysRevB.85.014104 PACS number(s): 77.55.−g

I. INTRODUCTION

Research of ferroelectric/piezoelectric perovskites has long been focused on the so-called "morphotropic" phase boundary (MPB), which describes a phase transition between tetragonal (T) and rhombohedral (R) symmetries induced by compositional changes. For instance, $Pb(Mg_{01/3},Nb_{2/3})O_3$ (PMN) or $Pb(Zn_{1/3}Nb_{2/3})O_3$ (PZN) is rhombohedral at room temperature and ambient condition but turns into a tetragonal phase when a critical amount of $PbTiO_3$ (PTO) (35% PTO for PMN and 9.5% PTO for PZN) is added. The charm of MPBs in ferroelectrics is the resultant high piezoelectricity that has been driving research into materials of this kind to further both scientific understanding[1–4] and technological applications.[5,6] The concept of MPB has been recently generalized and referred to the tetragonal-rhombohedral structural changes in pure compounds without compositional changes.[4,7,8] Rather than being triggered by compositional changes, the formation of MPBs in pure materials is due to the subjection to environmental changes such as temperature and pressure. Similar to composite ferroelectrics, pure materials at the T-R transition also exhibit large piezoelectricity.[4,9] The simplicity of pure materials provides more control over the experimental parameters, and allows more access to the structural details of the MPBs, and hence a better understanding of the correlations between their structures and corresponding ferroelectric/piezoelectric properties. Studies on single crystals have shown that MPBs are not abrupt but involve multiple monoclinic phases. For example, the lead-based perovskites at the MPBs first transform from the rhombohedral phase (with $R-3C$ symmetry) to a monoclinic Cm phase. They further change to another monoclinic phase (Cc) before turning into the tetragonal $P4mm$ phase.[7] While valuable information regarding the structures of MPBs could offered by experiments using single crystals and diffraction and/or spectroscopy techniques, direct access to ferroelectric/piezoelectric characterizations is limited in these experiments. A unique pathway to understand the detailed properties of MPBs has been recently developed using thin-film technology, which is capable of creating MPBs in ferroelectric thin films by large epitaxial strain.[8]

The model material in the aforementioned thin-film system is bismuth ferrite ($BiFeO_3$, BFO). It is a room-temperature multiferroic perovskite that exhibits coupled antiferromagnetism (Néel temperature: 643 K) with ferroelectric order (Curie temperature: 1103 K). BFO has attracted considerable attention because of its potential as a Pb-free ferroelectric material for advanced electronics and micro-electromechanical systems. Although the parent ground state of BFO is a rhombohedrally distorted perovskite ($R3c$), a tetragonally distorted phase with $a \sim 3.665$ Å and $c \sim 4.655$ Å has been reported.[10,11] The MPBs found in BFO thin films are caused by the large compressive epitaxial strain when grown on $LaAlO_3$ (LAO) substrates that has nearly 4.3% lattice mismatch with BFO. Interestingly, the MPBs in strained BFO thin films are physical boundaries that spatially separate the T-like and R-like phases and present self-organized, alternative, nanoscaled stripes in the mixed-phase region.[8] Structural studies later confirmed that both of the R-like and T-like phases possess monoclinic distortions and can be interswitched by applying electrical field.[12–14] It has been also found that the lattice structures of both phases are highly tilted at the mixed-phase region.[14] Like the single-crystal lead-based perovskites, MPBs in BFO thin films also involve the complicated R-M_A-M_C-T structural change.[15] Dupé *et al.* further proposed a tilted Cc monoclinic phase for the rhombohedral-like monoclinic M_A phase and a nontilted Cm monoclinic phase for the tetragonal-like M_C phase.[16] However, other groups such as Christen *et al.*[15] or Diéguez *et al.*[17] proposed another possible

 ©2012 American Physical Society

phase group of Pm for M_C and a Cc phase group for M_A and an intermediate $P1$ symmetry to make a continuous transition from M_A to M_C.[15,17] While the exact space groups of the M_A and M_C phase may change in different theoretical models, they are both ferroelectric and their polarizations concluded from these models are consistent: The ferroelectric polarizations in M_A and M_C are along $[xxz]$ and $[x0z]$, respectively. The ferroelectricity of the M_A and M_C phases has also been suggested to play an important role in the piezoelectric anomaly of perovskites assisting a process of polarization rotation under the morphotropic phase transition.

From a general perspective, the discovery of the coexistence of monoclinic R- and T-like phases in thin-film BFO paves the way for further understanding the properties of MPBs in perovskites. Although attempts to study the ferroelectric domains of BFO films with MPBs have been made, it remains technically challenging to probe the fine structures and, more importantly, the transition of the ferroelectric domains of the T-like and R-like phases by studying the striped mixed phases because of their nanoscaled, highly intimate nature. Therefore, alternative approaches to investigate strained BFO thin films are needed in order to explore the correlation between structural, ferroelectric, and piezoelectric properties of MPBs.

While previous studies focused mostly on the impacts of the thin-film thickness, which effectively change the strain state and result in the morphotropic phase transition, we show in this paper that using temperature as the experimental variable extends the dimension of the research and provides a more complete picture of the phase transition in strained BFO. We also notice that this approach creates additional controls of the MPBs in BFO thin films and offers an unprecedented platform for direct ferroelectric and piezoelectric measurements. Our results show that ferroelectric polarizations of BFO rotate when the thin film undergoes the M_C-M_A phase transition. Along with the polarization rotation, we also observed a piezoelectric anomaly at the transition and therefore directly confirm the correlation between the polarization rotation and the enhancement of piezoelectricity in ferroelectrics.

II. EXPERIMENTAL METHODS

Samples of epitaxial BFO thin films were prepared by RHEED-assisted pulsed laser deposition from a BFO target with 10% excess bismuth. Growth was carried out at 700 °C at oxygen pressure of 100 mTorr on single-crystal LAO (001) substrates. The growth rate was 3 nm/min at a laser rep-rate of 8 Hz. The final thickness of the BFO films was controlled by a combination of RHEED monitoring and deposition time. Following growth, the films were cooled at oxygen pressures of approximately 760 Torr. The topography of the films as well as their ferroelectric domain structures were studied at various temperatures with atomic force microscopy (AFM, Veeco Escope) and piezoelectric force microscopy (PFM). Tips used for PFM imaging were Ti-Pt coated cantilevers with an elastic constant of 4.5 N/m and a resonance frequency of 120 $\sim$ 190 kHz. When performing the PFM measurements, the scanning speed was set at 5 μm/s, the ac excitation frequency was 10.5 kHz, and the ac amplitude was 7 Vpp. Structural details of the samples were studied by high-resolution transmission electron microscopy (HR-TEM) and synchrotron-based x-ray diffraction (XRD) techniques. The reciprocal space maps (RSMs) of thickness-dependent experiments were performed using a PANalytical X'Pert Pro 4-circle x-ray diffractometer with Cu Kα_1 radiation (λ = 1.54 Å) and recorded by a series of θ-2θ scans with different ω offsets. These RSMs were then plotted in reciprocal lattice units Q (r.l.u.) (where $Q = \lambda/2d = \sin\theta$, $Q_x = Q \times \sin\beta$, and $Q_z = Q \times \cos\beta$, β is the offset angle = $\theta - \omega$). The temperature-dependent RSMs were collected at beamline BL-17B1 at the National Synchrotron Radiation Research Center (NSRRC) in Hsinchu, Taiwan. The incident beam was monochromated at 10 keV with a Si(111) double crystal mirror and then focused by a toroidal focusing mirror to get a higher intensity beam. Two sets of slits were placed before the samples to get the beam size about 0.3 × 0.7 mm and the other two were placed after the sample (or before the scintillation counter) to decrease background noises. Each map was measured step by step and plotted in the reciprocal lattice unit that is normalized to the LAO substrate (1 r.l.u. = $2\pi/a_{LAO}$). The counting rate of the RSM measurement was 2 $\sim$ 3 seconds per data point, depending on the temperature that is found to affect the signal-to-noise ratio. The overall measurement duration was around 6 $\sim$ 8 hours for one map.

III. RESULTS AND DISCUSSION

BFO thin films with various thicknesses (20–500 nm) were prepared on single-crystalline LAO (001) substrates and characterized by RSMs. Results of the evolution of

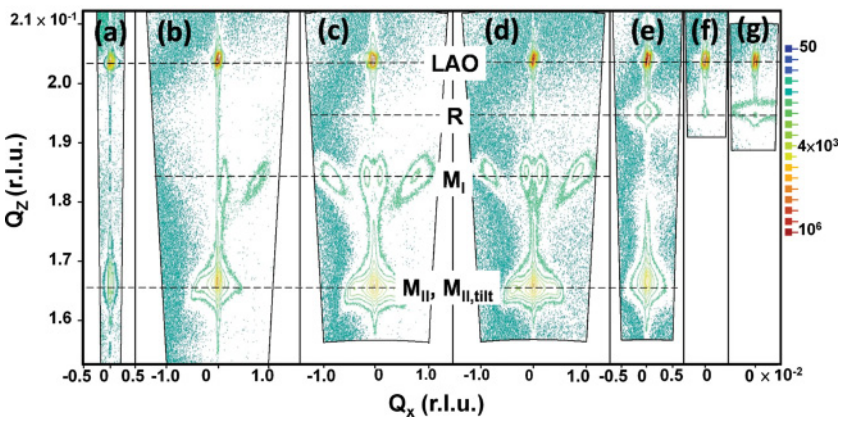

FIG. 1. (Color online) Reciprocal space maps from BFO films around the LAO (001) peak with thicknesses of (a) 20 nm, (b) 46 nm, (c) 77 nm, (d) 85 nm, (e) 165 nm, (f) 260 nm, and (g) 500 nm.

diffraction patterns from thin films with different thicknesses are shown in Figs. 1(a)–1(g), showing phase changes in thin films at different strain states. Notations adapted from previous studies,[14] which showed similar features, are used in Fig. 1. Peaks marked with "R" represent a monoclinically distorted rhombohedral bulklike phase ($c = 3.97$ Å); "M_I" refers to an intermediate monoclinic phase ($c = 4.16$ Å) at the mixed phase region according to previous studies as well as our TEM investigation (please see the Supplemental Material[18]); and "M_{II}" and "$M_{II,tilt}$" are monoclinically distorted tetragonal-like phases with an identical lattice constant ($c = 4.64$ Å), but one has the c axis normal to the substrate surface while the other has an off-normal c-axis orientation (marked with the subscription "tilt").[19]

In thin films with smaller thicknesses, e.g., 20 nm [Fig. 1(a)], only the M_{II} phase is observed. As thickness increases, e.g., 46 nm [Fig. 1(b)], the diffraction peaks associated with the M_I phase start to form, and the M_{II} peak also becomes wider, indicating the development of $M_{II,tilt}$ phase. When the film thickness reaches 77 nm, we observed two fully developed $M_{II,tilt}$ diffraction peaks, four M_I diffraction peaks, and the first evidence of the diffraction peak resulting from the R phase [Fig. 1(c)]. Similar features are also observed in the 85-nm thin film [Fig. 1(d)]. Further increase of the thickness relaxes the thin-film strain and causes loss of M_I and $M_{II,tilt}$ phases according to Fig. 1(e). No diffraction peaks from M_{II}, $M_{II,tilt}$, or M_I phases are observable in samples with thickness larger than 200 nm [Figs. 1(f) and 1(g)].

With the precise control of phases using different thin-film thicknesses, we chose the sample where the R phase just starts to emerge for the study of temperature-dependent phase transition in BFO. Figure 2 shows the temperature-dependent evolution of RSMs obtained from a 70-nm BFO thin film. At 200 °C, the M_I peaks are found to be further apart from each other in the H space, indicating the structure tilts further off the surface normal. Oppositely, the $M_{II,tilt}$ peaks move toward H = 0, showing a tendency to merge with the M_{II} peak at H = 0 [Fig. 2(b)]. At temperatures of 400 °C and beyond, peaks corresponding to M_I and $M_{II,tilt}$ phases are no longer observable [Figs. 2(c) and 2(d)], clearly showing a phase transition, at which the intermediate M_I and $M_{II,tilt}$ phases disappear, at 400 °C. In other words, the M_I and $M_{II,tilt}$ phases convert into the remaining phases, i.e., the R and M_{II} phases, at temperature higher than 400 °C. More details about the temperature-dependent phase evolutions of the M_I, M_{II}, and $M_{II,tilt}$ are revealed through their rocking curves of the (00L) reflections during a completed heating and cooling cycle. Figures 2(e) and 2(f) show that the tilting angles of M_I and $M_{II,tilt}$ phases both exhibit two gradations of structural variation but opposing trends during the heating or cooling processes. During the heating process, the tilting angle of M_I ($M_{II,tilt}$) phase slightly decreases (increases) until 200 °C and then increases (decreases) up to temperatures around 425 °C ± 25 °C. Above 450 °C, diffraction peaks from the two monoclinic phases are both hardly observable. The evolutions of the rocking curves of the M_I and $M_{II,tilt}$ phases are found to be completely reversible. During the cooling process, the M_I and $M_{II,tilt}$ diffraction peaks reappear at 400 °C and continue to grow as temperature further decreases. They completely revolve at the room temperature.

The morphology of the mixed phases in BFO at various temperatures (from room temperature up to 385 °C) studied by AFM is shown in Fig. 3. Color contrasts in these images represent the height profile of the surface, where the lower

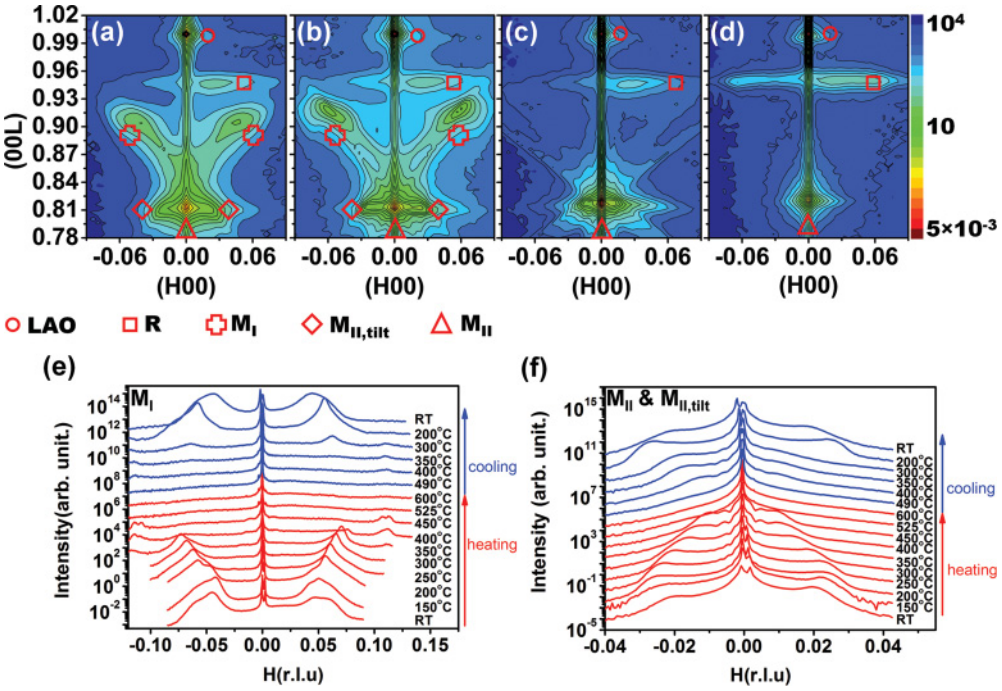

FIG. 2. (Color online) RSM results of BFO/LAO (001) taken at (a) 25 °C, (b) 200 °C, (c) 400 °C, and (d) 600 °C. Markers beside the XRD peaks indicate the presence of LAO, R-phase BFO, M_I-phase BFO, M_{II}-phase BFO, and $M_{II,tilt}$-phase BFO. (e) and (f) The rocking curves of M_I and M_{II} phases from the heating to cooling process, respectively.

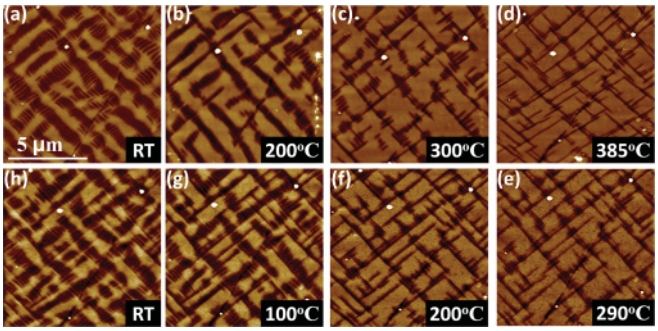

FIG. 3. (Color online) AFM topography of BFO thin films with mixed phases at various temperatures. Samples were imaged at (a) RT, (b) 200 °C, (c) 300 °C, (d) 385 °C, (e) 295 °C, (f) 200 °C, (g) 100 °C, and (h) RT. Images from (a) to (d) were taken during the heating process, while images from (e) to (h) were taken during the cooling process. All images were taken at the same area of the sample and have the same scan size.

(higher) regions are presented with dark (bright) contrast. Arrays of the dark striped regions at room temperature represent a periodic valley structure, which has been known to arise from the presence of intimately mixed M_{II}, R, M_I, and $M_{II,tilt}$ phases.[14] These stripelike features align into larger bands that lie orthogonally to each other [Fig. 3(a)]. Upon increasing the temperature of the sample to 200 °C, we observe a significant decrease in the width of the bands observed previously [Fig. 3(b)], while the band length remains essentially unaffected. Upon further increasing the temperature to 300 °C, it has been observed that these bands can be broken or truncated along the long axis [Fig. 3(c)]. Interestingly, upon reaching 385 °C we observed only thin and long strips evolving from the flat matrix, which is very different from the band feature observed at lower temperatures [Fig. 3(d)]. According to the RSM results [Fig. 2(c)], we know that these thin strips at 385 °C do not have either $M_{II,tilt}$ or M_I but consist only of the R phase, while the flat area that covers most of the surface is the M_{II} phase. We also found a reverse process when cooling the sample from 385 °C to 25 °C [Figs. 3(e)–3(h)], which echoes the observation of rocking-curve studies in the heating and cooling processes.

Important information drawn from the AFM results is that the dominate phase at high temperature is the M_{II} phase, and the structural change under the phase transition is caused by the conversions of M_I, $M_{II,tilt}$, and part of the R phase into the M_{II} phase. Since the phase transition between these monoclinic symmetries is the core of the structural change at MPBs, in-depth studies on the structural change of the M_{II} phase are necessary. We begin with $\theta-2\theta$ XRD investigations on the phase transition of the mixed-phase BFO from room temperature to 350 °C. Figure 4(a) shows that the intensity of the diffraction peak (L = 0.95) of the R phase becomes weaker at higher temperature, and slight shifts of the M_{II}-phase peak were observed. The weaker intensity of the XRD peak of the R phase is understandable because the R phase is more inclined from the surface normal and more broadened at higher temperature [as shown in Fig. 2(d)]. However, the shifts of the peak of the M_{II} phase post intriguing structural changes that could lead to a possible ferroelectric or antiferromagnetic transition, since these order parameters are coupled strongly in BFO.[20] The calculated *c*-axis parameters of BFO thin film (M_{II} phase) show a temperature dependence that is different from that of the LAO substrate: the *c*-axis parameter of the LAO substrate increases nearly linearly with the increase of temperature, but BFO shows a maximum in its *c*-axis parameter at around 150 °C [Fig. 4(b)].

The structural details of the M_{II} phase were further studied by RSMs around the (103) and (113) diffraction peaks. Previous RSM studies[12–15] have shown that BFO with monoclinic M_C symmetry exhibits a threefold split in the (103) peak and a twofold split of the (113) peak due to the shear angle along the [100] direction in M_C, while BFO with M_A symmetry exhibits a twofold split in the (103) XRD peak and a threefold split in the (113) XRD peak due to the shear angle along the [110] direction in M_A [Fig. 5(a)]. We have performed (100) and (110) XRD reflections in the (H0L) and (HHL) scattering zones at room temperature, 150 °C, and 200 °C. At room temperature, the BFO sample displays a threefold split of the (103) diffraction peak and a twofold split of the (113) peak, manifesting an M_C phase with lattice parameters $a = 3.81$ Å, $b = 3.76$ Å, $c = 4.64$ Å, and a shear angle, $\beta_{MC} = 88.5°$ [Figs. 5(b) and 5(c)]. RSMs of the same sample at 150 °C exhibit very different patterns [Figs. 5(d) and 5(e)]: a twofold split in the (103) peak and a threefold split in the (113) peak, showing an M_A phase with lattice parameters $a = 3.80$ Å, $b = 3.79$ Å, $c = 4.66$ Å, and $\beta_{MA} = 86.8°$.

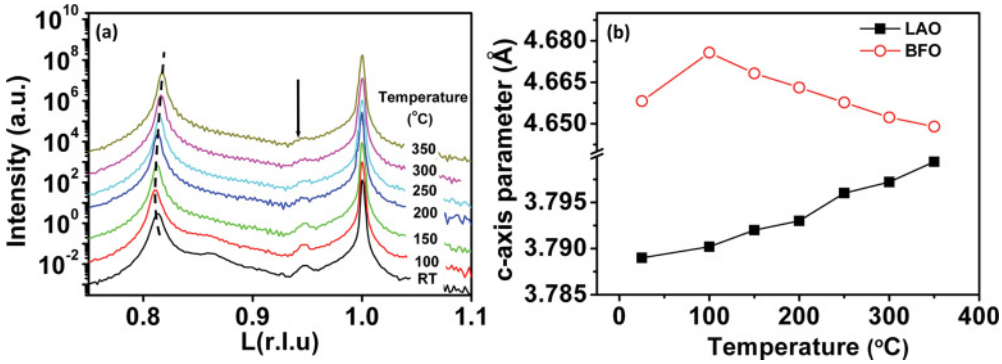

FIG. 4. (Color online) (a) X-ray normal scan of a BFO thin film with reference to LAO (001) peaks at various temperatures. The dashed line is used as a guide to visualize the shifts of the M_{II} peaks. The arrow marks the R peaks. (b) *c*-axis lattice parameters of BFO (001) and LAO (001) from RT to 350 °C.

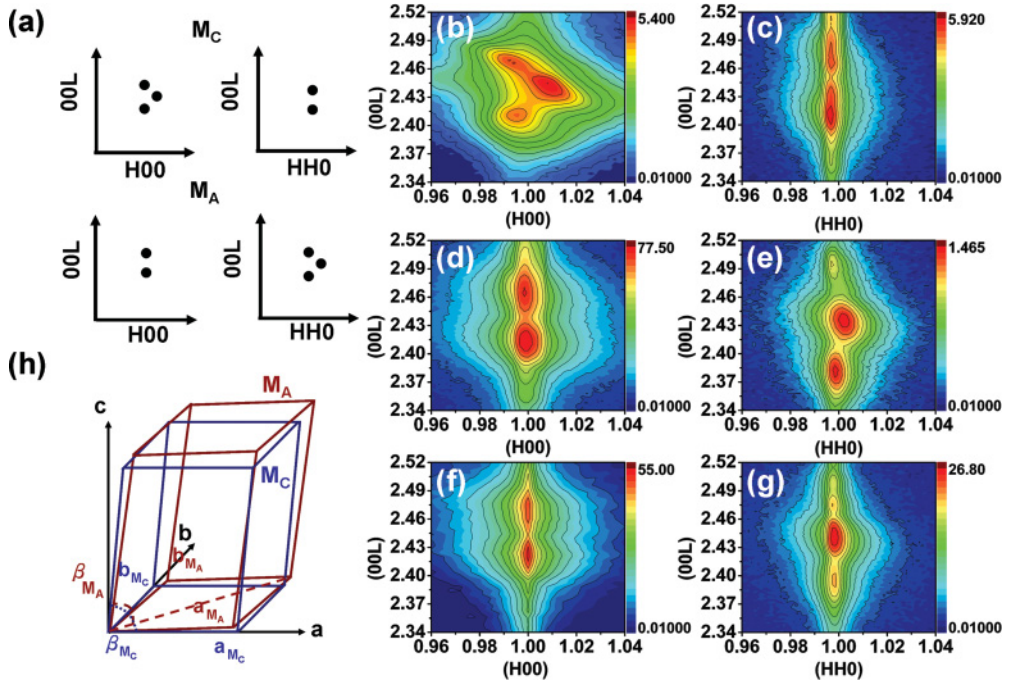

FIG. 5. (Color online) (a) Schematics of expected XRD peaks of M_A and M_C phases in the (H0L) and (HHL) scattering zones of an RSM. (b) and (c) Experimental RSMs of (103) and (113) of our BFO thin film at RT. (d) and (e) The RSMs of (103) and (113) of the BFO thin film at 150 °C. (f) and (g) The RSMs of (103) and (113) of the BFO thin film at 200 °C. (h) Schematics of the lattice structures of the M_C (blue) and the M_A (red) phases of the BFO thin films at the phase transition temperature.

Only slight changes in the RSM patterns of M_A phase at 200 °C were observed, as shown in Figs. 5(f) and 5(g), resulting in a small variation for the structural parameters ($a = 3.80$ Å, $b = 3.80$ Å, $c = 4.65$ Å, and $\beta_{MA} = 87.7°$). The evolution of RSM patterns from 25 °C to 200 °C confirms that the maximum of the *c*-axis lattice parameter found in the M_{II} phase at around 150 °C [Fig. 4(b)] is actually a phase transition from a low-temperature phase (i.e., the M_C phase) to a high-temperature phase (i.e., the M_A phase) in the sample. Two sets of symmetries have been theoretically proposed for the ground-state phase of highly compressive strained BFO thin films. One is the *Pm*, or *Cm* symmetry, where the shear orientation is along the [100] direction.[15,17] The other is the *Cc* symmetry, where the shear orientation is along the [110] direction.[21] Our experimental results suggest that depending on temperature the ground-state phase of strained BFO thin films changes its symmetry from *Pm* or *Cm* (the M_C phase) at low temperature to C_C (the M_A phase) at high temperature.

The observed M_C-M_A transition provides new insights into the R, M_{II}, $M_{II,tilt}$, and M_I phases at different temperatures. First, the M_{II} phase does *not* preserve its symmetry throughout the temperature variation. Its symmetry actually changes from M_C to M_A, but its *c*-axis lattice parameter is essentially kept the same (except the maximum observed at around 150 °C). Second, the M_{II} phase, to which M_I, $M_{II,tilt}$, and R phases are converted at elevated temperature, possesses the M_A symmetry, not the M_C symmetry. It is also noteworthy that the M_A phase observed at around 150 °C in this experiment is different from those observed in samples made on substrates with less lattice mismatch, e.g., $SrTiO_3$ (STO). BFO thin films grown on STO with biaxial strain exhibit an M_A phase and possess a monoclinic-distorted rhombohedral-like structure with a *c*-axis parameter close to that of the bulk BFO (~3.965 Å).[22,23] However, the M_A phase observed in our work has a very large *c*-axis parameter (>4.6 Å), which is close to the *c*-axis parameter of the tetragonal BFO but still has rhombohedral-like features, e.g., an inclined angle toward [110] [Fig. 5(h)]. We attribute the exceptionally large c/a ratio (~1.2) of the M_A phase to two competing mechanisms. On the one hand, the expansion of the LAO lattice parameters at high temperature triggers the formation of M_A phase by reducing the compressive strain in BFO, and on the other hand the thermodynamic stability of compressively stressed BFO favors the tetragonal distortion at high temperature according to the

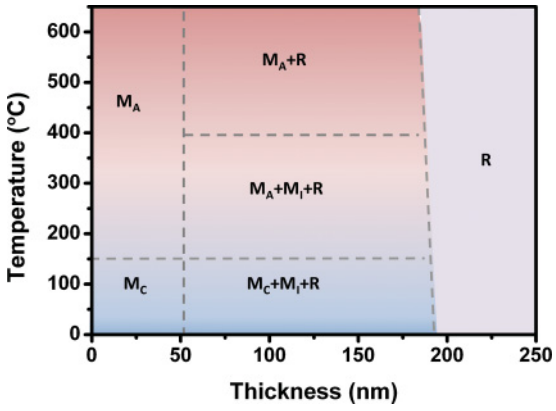

FIG. 6. (Color online) Thickness-temperature phase diagram of compressively strained BFO thin films.

phase-field model.[8] A balance between these two tendencies results in a structure that has an M_A symmetry but a large *c*-axis lattice parameter. However, further experimental and theoretical studies on this system are required to gain more details.

The interesting, but highly complicated, phase evolution of compressively strained BFO thin films observed in our experiments can be further clarified in a thickness-temperature phase diagram (Fig. 6). Thin films with thickness less than 50 nm (highly strained) have an M_C phase at temperatures below 150 °C but change to M_A at higher temperatures. For thin films with thickness larger than ~200 nm (highly relaxed), the dominant phase is the R phase. Thin films with thicknesses between 50 and 200 nm (partially relaxed) have multiple phases and complicated structural changes with temperature: below 150 °C, they consist of M_C, M_I, and R phases; from 150 °C to 400 °C, they consist of M_A, M_I, and R phases; and at 400 °C and above, they consist of M_A and R phases.

The fact that the monoclinic phase transition occurs across the entire sample surface (even at the smooth area outside the striped regions) at temperatures *slightly above* the room temperature in *ambient* condition provides a unique opportunity to study the ferroelectric and piezoelectric properties of perovskites at morphotropic phase. As shown by the schematics in Figs. 7(a) and 7(b), ferroelectric polarizations of M_C and M_A phases are known to lie on the {100} and {110} planes, respectively. It has also been suggested that ferroelectric polarization rotates between the {100} and {110} planes during the M_C-to-M_A transition.[24–26] To manifest the polarization rotational dynamics, the phase and amplitude images have been used simultaneously to study the variation of piezoresponse signals (X), which is given by

$$X = A \times \cos(P), \tag{1}$$

where A is amplitude signals and P is phase signals. Therefore there should be three kinds of piezoresponse signals like the colored arrows in Fig. 7(a) if the cantilever is aligned in the [100] direction in the case of the M_C phase. The first is that polarization is parallel to the cantilever, with $A = 0$ (dark contrast in amplitude images) and $P = 0^o$ or 180^o (dark and bright contrasts in phase images, respectively). The second is that polarization is perpendicular to the cantilever, with $A =$ maximum (bright contrast in amplitude images) and $P = 0^o$ (dark contrast in phase images). The last is that polarization is also perpendicular to the cantilever but with opposite phase, with $A =$ maximum (bright contrast in amplitude images) and $P = 180^o$ (bright contrast in phase images). On the other hand, only two kinds of piezoresponse signals like the white and dark arrows in Fig. 7(b) can be observed in the case of M_A phase if we follow this logic. These two signals will have no difference in the amplitude strength but opposite phases.

We now return to the temperature-dependent PFM measurements. Surface topography at room temperature shows an atomically smooth morphology [Fig. 7(c)], while the IP-PFM shows a stripelike feature when scanning the sample along the [100] direction [Figs. 7(d) and 7(e)]. The stripes are formed due to the combination of the three kinds of in-plane piezoresponse signals discussed above to minimize the electrostatic energy of the domains.[13,27,28] Two are perpendicular to the scanning

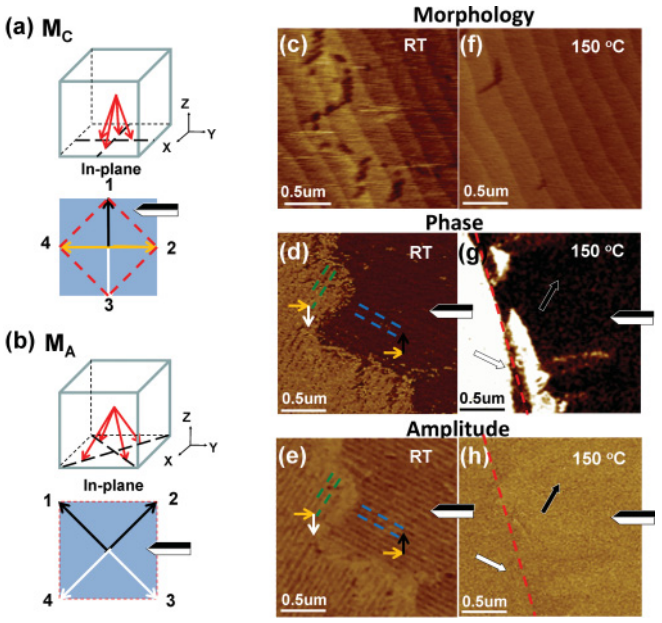

FIG. 7. (Color online) (a) Schematics of the ferroelectric polarizations in M_C, which shows four in-plane polarization variants on the {100} planes. Three contrasts (dark, light, and brown) are expected from PFM measurements when the cantilever is aligned to [100]. (b) Schematics of the ferroelectric polarizations in M_A. The polarization of M_A lies on the {110} plane, also resulting in four in-plane polarization variants. However, when conducting PFM measurements with the cantilever aligned to [100], two contrasts (dark, light) are expected. (c) AFM, (d) PFM phase, and (e) PFM amplitude images of a BFO sample at RT with the cantilever aligned to [100]. (f) AFM, (g) PFM phase, and (h) PFM amplitude images of the same scanning area as shown in (c)–(e) but at 150 °C. The cantilever is also aligned to [100]. The white, black, and brown arrows in (d), (e), (g), and (h) indicate the directions of the in-plane polarization.

direction and have the same stronger amplitudes as both are displayed in brighter contrast in Fig. 7(e). These two polarizations can be distinguished by their opposite phases, presented in the bright and dark contrasts in Fig. 7(d). The other is parallel to the cantilever and with the weaker amplitude, as displayed in dark brown color in Fig. 7(e). The PFM results are consistent with the expected result from the M_C phase, as depicted in Fig. 7(a). Repeating the same AFM and PFM measurements over the same area at 150 °C shows that while the stepwise topography remains intact [Fig. 7(f)], the in-plane PFM shows a puddlelike feature with a stark contrast between dark and light in the phase image [Fig. 7(g)] and shows no obvious contrast in the amplitude image [Fig. 7(h)]. This indicates that the in-plane polarization of the sample has changed its direction from [100] to [110], which is expected from the M_A phase shown in Fig. 7(b). The observed change in in-plane polarization direction from [100] to [110] at elevated temperature confirms the polarization rotation in BFO when the thin film undergoes a phase transition from M_C to M_A.

We also studied the longitudinal (d_{33}) piezoelectric hysteresis loops of the M_C and M_A phases at different temperatures [Fig. 8(a)]. Results show that d_{33} at temperatures below 100 °C is around 50 pm/V but increases to 66.1 pm/V at

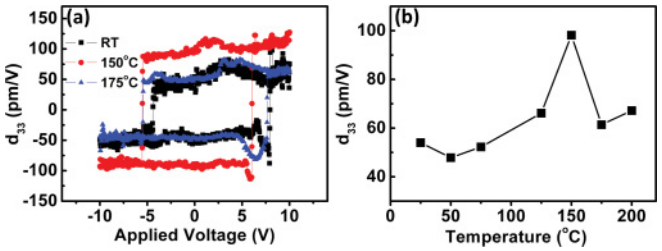

FIG. 8. (Color online) (a) Piezoelectric response loops of the BFO thin films at RT, 150 °C, and 175 °C. (b) Variation of d_{33} against temperature.

125 °C [Fig. 8(b)]. Upon further increase of temperature to 150 °C, a large d_{33} (98.1 pm/V) is observed. Further increases of temperature show reductions in d_{33} to 61.4 pm/V (175 °C) and 67.2 pm/V (200 °C). The temperature (150 °C) at which the d_{33} anomaly is observed matches the results of XRD and PFM studies and hence can be understood as a result of the combination of structural change and the polarization rotation. In more detail, our sample shows a steady piezoelectric response at around 50 or 60 pm/V when it is in a stable phase of either M_C or M_A. This is typical for BFO thin films under compressive strain.[29] However, in the regime of phase transition, both the lattice structure and ferroelectric polarization have additional degrees of freedom to respond to the external electrical field. The BFO lattices are allowed to tilt along the [100] and [110] directions [Fig. 5(h)], and the ferroelectric dipole can exercise in-plane rotation between the [100] and [110] directions. The consistency of the structural, ferroelectric, and piezoelectric properties observed in our experiments provide direct experimental proof that the polarization rotation induced by the structural transition gives rise to the enhancement of piezoelectric response typically observed in ferroelectrics with MPBs.

IV. CONCLUSION

In summary, a full picture of the morphotropic phase transition has been provided by our detailed study on compressively strained BFO thin films. Precise control of material structures by varying the thin-film thickness and temperature has been demonstrated. The lattice structure is found to be very sensitive to temperature and multiple phase transitions are observed. We found the dominant phase at room temperature possesses an M_C symmetry but switches to an M_A symmetry at a characteristic temperature of 150 °C. The c-axis parameter of the M_A phase at the transition temperature is found to be very large and close to that of tetragonal BFO. This structural change is accompanied by a ferroelectric polarization rotation from $[x0z]$ to $[xxz]$. The piezoelectric response is also enhanced considerably during the phase transition. Our studies directly confirm that the high piezoelectric response (d_{33}) in BFO with MPBs is due to structural instability and polarization rotation at the phase transition. Our results provide key insights into ferroelectric materials and could help future engineering of highly piezoelectric thin films.

ACKNOWLEDGMENT

Financial support from the National Science Council through Projects No. NSC 99-2112-M-006-012-MY3 and No. NSC 99-2811-M-009-003 is gratefully acknowledged by the authors.

[1] B. Jaffe, W. R. Cook, and H. Jaffe, *Piezoelectric Ceramics* (Academic Press, London, 1971).
[2] M. J. Haun, E. Furman, S. J. Jang, and L. E. Cross, Ferroelectrics **99**, 13 (1989).
[3] D. Vanderbilt and M. H. Cohen, Phys. Rev. B **63**, 094108 (2001).
[4] H. Fu and R. E. Cohen, Nature (London) **403**, 281 (2000).
[5] M. E. Lines and A. M. Glass, *Principles and Applications of Ferroelectrics and Related Materials* (Clarendon Press, Oxford, 1979).
[6] K. Uchino, *Piezoelectric Actuators and Ultrasonic Motors* (Kluwer Academic, Boston, 1996).
[7] M. Ahart, M. Somayazulu, R. E. Cohen, P. Ganesh, P. Dera, H.-K. Mao, R. J. Hemley, Y. Ren, P. Liermann, and Z. Wu, Nature (London) **451**, 545 (2008).
[8] R. J. Zeches, M. D. Rossell, J. X. Zhang, A. J. Hatt, Q. He, C.-H. Yang, A. Kumar, C. H. Wang, A. Melville, C. Adamo, G. Sheng, Y.-H. Chu, J. F. Ihlefeld, R. Erni, C. Ederer, V. Gopalan, L. Q. Chen, D. G. Schlom, N. A. Spaldin, L. W. Martin, and R. Ramesh, Science **326**, 977 (2009).
[9] Z. Wu and R. E. Cohen, Phys. Rev. Lett. **95**, 037601 (2005).
[10] D. Ricinschi, K.-Y. Yun, and M. Okuyama, J. Phys.: Condens. Matter **18**, L97 (2006).
[11] H. Béa, B. Dupé, S. Fusil, R. Mattana, E. Jacquet, B. Warot-Fonrose, F. Wilhelm, A. Rogalev, S. Petit, V. Cros, A. Anane, F. Petroff, K. Bouzehouane, G. Geneste, B. Dkhil, S. Lisenkov, I. Ponomareva, L. Bellaiche, M. Bibes, and A. Barthélémy, Phys. Rev. Lett. **102**, 217603 (2009).
[12] D. Mazumdar, V. Shelke, M. Iliev, S. Jesse, A. Kumar, S. V. Kalinin, A. P. Baddorf, and A. Gupta, Nano Lett. **10**, 2555 (2010).
[13] Z. Chen, Z. Luo, C. Huang, Y. Qi, P. Yang, L. You, C. Hu, T. Wu, J. Wang, C. Gao, T. Sritharan, and L. Chen, Adv. Funct. Mater. **21**, 133 (2011).
[14] A. R. Damodaran, C.-W. Liang, Q. He, C.-Y. Peng, L. Chang, Y.-H. Chu, and L. W. Martin, Adv. Mater. **23**, 3170 (2011).
[15] H. M. Christen, J. H. Nam, H. S. Kim, A. J. Hatt, and N. A. Spaldin, Phys. Rev. B **83**, 144107 (2011).
[16] B. Dupé, I. C. Infante, G. Geneste, P.-E. Janolin, M. Bibes, A. Barthélémy, S. Lisenkov, L. Bellaiche, S. Ravy, and B. Dkhil, Phys. Rev. B **81**, 144128 (2010).
[17] O. Diéguez, O. E. González-Vázquez, J. C. Wojdeł, and J. Íñiguez, Phys. Rev. B **83**, 094105 (2011).
[18] See Supplemental Material at http://link.aps.org/supplemental/10.1103/PhysRevB.85.014104 for detailed structural investigation of morphotropic phase boundary (MPB) by TEM, AFM, and RSM measurements.

[19]Z. Chen, S. Prosandeev, Z. L. Luo, W. Ren, Y. Qi, C. W. Huang, L. You, C. Gao, I. A. Kornev, T. Wu, J. Wang, P. Yang, T. Sritharan, L. Bellaiche, and L. Chen, Phys. Rev. B. **84**, 094116 (2011).

[20]I. C. Infante, J. Juraszek, S. Fusil, B. Dupe, P. Gemeiner, O. Dieguez, F. Pailloux, S. Jouen, E. Jacquet, G. Geneste, J. Pacaud, J. Iniguez, L. Bellaiche, A. Barthelemy, B. Dkhil, and M. Bibes, Phys. Rev. Lett. **107**, 237601 (2011).

[21]A. J. Hatt, N. A. Spaldin, and C. Ederer, Phys. Rev. B **81**, 054109 (2010).

[22]D. H. Kim, H. N. Lee, M. D. Biegalski, and H. M. Christen, Appl. Phys. Lett. **92**, 012911 (2008).

[23]H. W. Jang, S. H. Baek, D. Ortiz, C. M. Folkman, R. R. Das, Y. H. Chu, P. Shafer, J. X. Zhang, S. Choudhury, V. Vaithyanathan, Y. B. Chen, D. A. Felker, M. D. Biegalski, M. S. Rzchowski, X. Q. Pan, D. G. Schlom, L. Q. Chen, R. Ramesh, and C. B. Eom, Phys. Rev. Lett. **101**, 107602 (2008).

[24]B. Noheda, D. E. Cox, G. Shirane, S.-E. Park, L. E. Cross, and Z. Zhong, Phys. Rev. Lett. **86**, 3891 (2001).

[25]L. Bellaiche, A. García, and D. Vanderbilt, Phys. Rev. Lett. **84**, 5427 (2000).

[26]J. Kiat, Y. Uesu, B. Dkhil, M. Matsuda, C. Malibert, and G. Calvarin, Phys. Rev. B **65**, 064106 (2002).

[27]N. Balke, S. Choudhury, S. Jesse, M. Huijben, Y.-H. Chu, A. P. Baddorf, L. Q. Chen, R. Ramesh, and S. V. Kalinin, Nat. Nanotechnol. **4**, 868 (2009).

[28]Z. Chen, Z. Luo, Y. Qi, P. Yang, S. Wu, C. Huang, T. Wu, J. Wang, C. Gao, T. Sritharan, and L. Chen, Appl. Phys. Lett. **97**, 242903 (2010).

[29]J. X. Zhang, B. Xiang, Q. He, J. Seidel, R. J. Zeches, P. Yu, S. Y. Yang, C. H. Wang, Y.-H. Chu, L. W. Martin, A. M. Minor, and R. Ramesh, Nat. Nanotechnol. **6**, 98 (2011).